Giant Birefringent Optics in Multilayer Polymer Mirrors

Michael F. Weber, Carl A. Stover, Larry R. Gilbert, Timothy J. Nevitt, Andrew J. Ouderkirk*

Multilayer mirrors that maintain or increase their reflectivity with increasing incidence angle can be constructed using polymers that exhibit large birefringence in their indices of refraction. The most important feature of these multilayer interference stacks is the index difference in the thickness direction (z axis) relative to the in-plane directions of the film. This z-axis refractive index difference provides a variable that determines the existence and value of the Brewster's angle at layer interfaces, and it controls both the interfacial Fresnel reflection coefficient and the phase relations that determine the optics of multilayer stacks. These films can yield optical results that are difficult or impossible to achieve with conventional multilayer optical designs. The materials and processes necessary to fabricate such films are amenable to large-scale manufacturing.

There are two conventional ways to create a mirror: using the surface of a layer of metal, or using a tuned interference stack composed of multiple layers of transparent dielectric materials. Metal mirrors are inexpensive and perform robustly across a broad range of angles, wavelengths, and polarizations, but they exhibit limited reflectivity. Multilayer interference mirrors are routinely used for optical applications requiring high reflectivity and wavelength selectivity. Although they can be designed to achieve a wide range of optical characteristics, each design typically performs across a limited range of incidence angles, wavelengths, and polarizations. A key limitation of multilayer mirrors stems from Brewster's law, a nearly 200-year-old maxim of optics, which predicts the decrease of reflection for p-polarized light at material interfaces with increasing incidence angle. Specifically, Brewster's law states that there is an angle of incidence (Brewster's angle) for which the reflectivity for p-polarized light vanishes at a material interface. As a result, a multilayer interference mirror that is designed to have a 1% loss for reflection of p-polarized light (99% reflectivity) at normal incidence can have many times that loss at high incidence angles.

Using highly birefringent polymers, we have found that multilayer mirrors can be constructed that maintain or increase their reflectivity with increasing incidence angle. The reflective characteristics of these mirrors require a generalization of Brewster's law. This generalization has enabled the development of a new class of multilayer interference optics with design freedoms that can result in unprecedented means for transporting, filtering, and reflecting light.

3M Film/Light Management Technology Center, 3M Center, St. Paul, MN 55144, USA.

*To whom correspondence should be addressed. E-mail: 3mopticalfilm@mmm.com

Optical birefringence describes the difference of a material's refractive index with direction. When birefringence is on the order of the change of the in-plane refractive index between adjacent material layers, surprising and useful optical effects occur. We refer to these effects as giant birefringent optics (GBO). A central feature of GBO is improved control of the reflectivity of p-polarized light. With the additional design freedom allowed by GBO, Brewster's angle can be controlled to any angle from 0° (normal incidence) to 90° (grazing incidence), to imaginary values for light incident from media of any index of refraction. For imaginary values of Brewster's angle, the reflectivity at material interfaces (referred to as Fresnel or interfacial reflectivity) for p-polarized light increases with angle of incidence in a similar or identical form to that for s-polarized light. By comparison, isotropic materials have no substantial optical birefringence; that is, their refractive index values are equal for all directions. Interfaces of these conventional isotropic materials exhibit a limited range of Brewster's angles.

Because the optical effects presented are based on the fundamental physics of interfacial reflection and phase thickness and not on a particular multilayer interference stack design, new design freedoms are possible. For example, designs for wide-angle, broadband applications are simplified if optical elements with no Brewster's angle are used, particularly if immersed in a high-index medium such as a glass prism. Color filters can be designed that provide high color saturation at all incidence angles and polarizations. Alternatively, a mirror or reflecting polarizer can be designed to have a Brewster's angle that is accessible in air.

Conventional polymer film-making processes have been enhanced to fabricate a wide array of GBO films from commercially available polymers and monomers for use in a range of applications. These applications include high-efficiency mirrors for piping visible light over long distances or uniformly lighting small optical displays. GBO multilayer films have been used to create reflective polarizers that make liquid crystal displays brighter and easier to view. Other applications include decorative products, cosmetics, security films, optoelectronic components, and infrared solar control reflectors for architectural and automotive glazing. After a review of birefringent optics, we discuss the relations describing GBO and show the implications of GBO on optical film performance and applications.

Background. Multilayer interference optics can generally be described as the use of the amplitudes and phases of light reflected at planar material boundaries to produce constructive and destructive interference effects. Pairs or groupings of adjacent layers (termed unit cells) can produce constructive interference effects when their thicknesses are properly scaled to the wavelengths of interest. These interference effects in multilayered structures result in the development of wavelength regions of high reflectivity (reflection bands) with adjacent wavelength regions of high transmission (pass bands) (*1*).

Much of the design effort in multilayer interference optics is devoted to controlling the angular dependence of reflection bands, which is complicated by polarization effects. These effects have long been known, with publications dating to before the turn of the century [see, e.g., Drude (*2, 3*)]. Sir David Brewster empirically deduced the law named for him by observing that light reflected from an air-glass interface is highly polarized at a specific angle (*4*). The same phenomenon occurs for all interfaces between isotropic materials. Aside from the well-known MacNeille polarizing beamsplitters (*5*) and magneto-optic materials (*6*), such polarization effects are typically undesirable, as they limit the angular performance of multilayer interference stacks. Various researchers (*7–10*) have developed a variety of limited solutions to the problem. In addition, modern computer optimization codes have dealt admirably with the problem. However, the basic phenomenon associated with Brewster's angle still continues to constrain the angular and wavelength performance of multilayer interference stacks fabricated from materials having isotropic indices of refraction.

Multilayer polymeric interference mirrors were pioneered in the late 1960s (*11*), and even though the large birefringence of oriented polyethylene terephthalate (PET) was known at the time (*12*), the use of materials with large optical birefringence in a multilayer mirror (polymeric or otherwise) has not been reported. Numerous other works have been published on birefringent optical materials (*13–18*), but none of these discuss the use of birefringence to control (or eliminate) Brewster's angle effects and phase thickness relations among interfaces in multilayer interference stacks.

Giant birefringent optics. The coordinate system used to reference the material axes and the incident electric field for different linear polarization states is shown in Fig. 1. For GBO, each birefringent layer is either uniaxial, with its *z*-direction index different from the equal in-plane indices (equal *x*-*y* direction indices), or biaxial, with the *x*-, *y*-, and *z*-direction indices all being unequal.

Part of the optical behavior of a multilayer interference stack originates in the angular dependence of the Fresnel interface reflection coefficients, including the nature of the Brewster's angle θ_B. Figure 2 compares the magnitudes of Fresnel reflection for various internal interfaces (that is, between materials 1 and 2 in Fig. 1) as a function of angle of incidence (from the external medium). For convenient comparison of material pairs having a range of index differences, all of the reflectance values plotted for a given material interface have been normalized to their value at normal incidence. An external medium with a refractive index $n_0 = 1.60$ (e.g., a glass prism) is chosen so that a wide range of propagation angles can be explored. Snell's law requires that the larger the external medium index, the greater the range of propagation angles that can be achieved within the films. For most isotropic material pairs, θ_B is not accessible for light incident from air.

Curve c in Fig. 2 shows the interfacial reflectivity for a common material pair used in the multilayer interference film industry, SiO_2-TiO_2, which in this case has $\theta_B = 52°$. The range of θ_B for other commonly used isotropic material pairs that are transparent in the visible portion of the spectrum is indicated by the shaded portion of the plot (about 40° to 70° in a $n_0 = 1.60$ medium); the lower bound of 40° occurs for a material pair with indices 1.35 and 1.50 and the upper bound for a pair with indices 1.95 and 2.4. Tellurium-polystyrene, an interesting material system that is transparent only at mid-infrared wavelengths, was recently reported by Fink *et al.* (*19*) and is represented by curve d; in this case it has $\theta_B = 71°$ (similar to ZrO_2-TiO_2).

These examples illustrate behavior that is indeed a "law" for interfaces between two isotropic materials, regardless of the incident me-

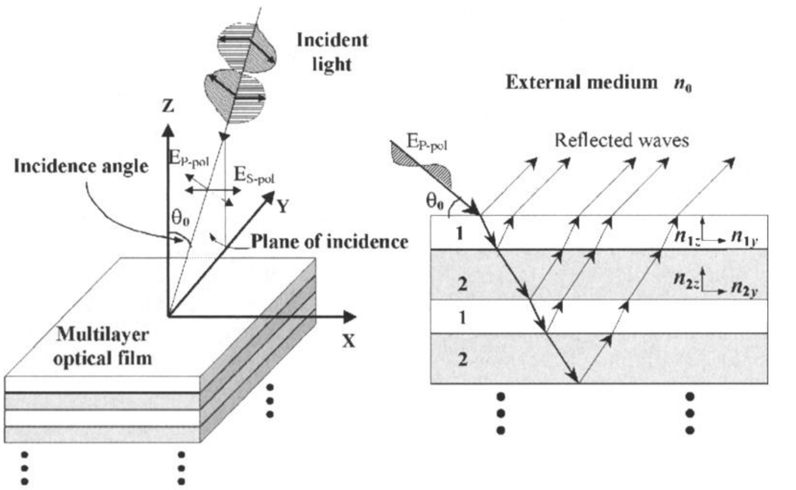

Fig. 1. The normal conventions for polarization are followed here, with p-polarized light having its electric field in the plane of incidence and s-polarized light with its electric field perpendicular to the plane of incidence. The *y* and *z* directions in the layer are shown. Note that only p-polarization interacts with the indices along the *z* axis of the layer. For clarity, only the resultant reflected waves are indicated in the right-side diagram.

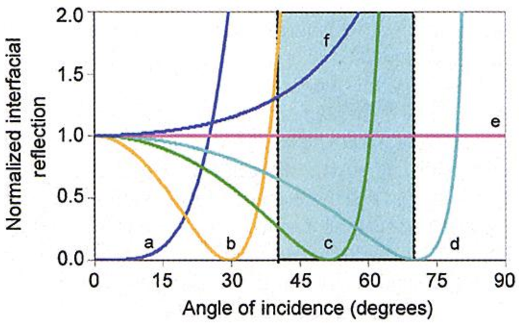

Fig. 2. In order of increasing θ_B, curves a through f illustrate p-polarized interfacial reflectivity for the following sets of indices: (a) GBO $n_{1y} = 1.63$, $n_{1z} = 1.5$, $n_{2y} = 1.63$, $n_{2z} = 1.63$ (birefringent polyester–isotropic polyester), $\theta_B = 0°$; (b) GBO $n_{1y} = 1.54$, $n_{1z} = 1.63$, $n_{2y} = 1.5$, $n_{2z} = 1.5$ (syndiotactic polystyrene–PMMA), $\theta_B = 30°$; (c) Isotropic $n_{1y} = 2.4$, $n_{1z} = 2.4$, $n_{2y} = 1.46$, $n_{2z} = 1.46$ (TiO_2-SiO_2), $\theta_B = 52°$; (d) Isotropic $n_{1y} = 5.0$, $n_{1z} = 5.0$, $n_{2y} = 1.58$, $n_{2z} = 1.58$ (tellurium-polystyrene), $\theta_B = 71°$; (e) GBO $n_{1y} = 1.8$, $n_{1z} = 1.5$, $n_{2y} = 1.5$, $n_{2z} = 1.5$ (birefringent polyester–PMMA), θ_B is imaginary; and (f) GBO $n_{1y} = 1.8$, $n_{1z} = 1.5$, $n_{2y} = 1.56$, $n_{2z} = 1.56$ (birefringent polyester–isotropic polyester), θ_B is imaginary. The shaded portion indicates the range of θ_B for isotropic material pairs that are transparent in the visible portion of the spectrum.

dium index. From its value for normally i dent light, the interfacial reflection for p-p ized light decreases monotonically with incr ing incidence angle up to θ_B (*20*). Whether θ observed depends on the range of propaga angles that are accessible in the materials determined by Snell's law of refraction and incident medium index.

Curves a, b, e, and f in Fig. 2 repre interfacial reflection of various birefringent terial pairs from which we have fabricated r tilayer interference stacks. Curve e is for special case of matched *z*-direction ind where reflectivity is constant with angle o cidence. When the interface materials ha *z*-direction index difference Δn_z of opposite relative to the in-plane index difference Δn_y, interfacial reflection behavior for p-polar light is similar to that for s-polarized light (c f). The material pairs used for curves a ar demonstrate that θ_B can be reduced to any va including 0°, by the appropriate choice o direction index values relative to the in-p indices.

The quantitative relations that provide basis for GBO offer physical insight into optical effects that are achievable with b fringent multilayer stacks. These are cussed below.

Fresnel coefficients and phase relati for GBO. At the boundary between two refringent materials 1 and 2 that have t orthogonal optic axes coincident with film axes (see Fig. 1), the Fresnel reflec coefficient for p-polarized light propaga from material layer 1 into material layer 2 be found in textbooks (*21*) and is given l

$$r_p = \left(n_{2z}n_{2y}\sqrt{n_{1z}^2 - n_0^2 \sin^2\theta_0} - n_{1z}n_{1y}\sqrt{n_{2z}^2 - n_0^2\sin^2\theta_0} \right) \Big/ \left(n_{2z}n_{2y}\sqrt{n_{1z}^2 - n_0^2\sin^2\theta_0} + n_{1z}n_{1y}\sqrt{n_{2z}^2 - n_0^2\sin^2\theta_0} \right)$$

where n_0 and θ_0 refer to the index and angl the external isotropic medium, respectively the limit of isotropic indices, Eq. 1 reduce that given by Born and Wolf (*22*). For suc material system, s-polarized light interacts c with the in-plane indices and the Fresnel c ficient is the same as for isotropic material:

$$r_s = \frac{\sqrt{n_{1x}^2 - n_0^2\sin^2\theta_0} - \sqrt{n_{2x}^2 - n_0^2\sin^2\theta_0}}{\sqrt{n_{1x}^2 - n_0^2\sin^2\theta_0} + \sqrt{n_{2x}^2 - n_0^2\sin^2\theta_0}}$$

In Eqs. 1 and 2, the plane of incidence (see 1) is taken to be along the *y* axis. If the plan incidence were along the *x* axis, the values o and n_y would be exchanged in Eqs. 1 and 2. uniaxial material systems, $n_x = n_y$.

By inspection, we can arrive at the effective interfacial indices for the ith layer of a birefringent material:

$$n_{is}^{int} = \frac{\sqrt{n_{ix}^2 - n_0^2 \sin^2 \theta_0}}{\cos \theta_0} \tag{3}$$

for s-polarized light and

$$n_{ip}^{int} = \frac{n_{iy} n_{iz} \cos \theta_0}{\sqrt{n_{iz}^2 - n_0^2 \sin^2 \theta_0}} \tag{4}$$

for p-polarized light. Effective indices are useful in that they combine angle and polarization effects into a simple expression with the form of a refractive index. Equation 4 leads to a generalized version of Brewster's law that can be used to solve for θ_B, the incidence angle for which

$$n_{1p}^{int} = n_{2p}^{int} \tag{5}$$

There are some interesting limits to Eq. 1. For the case of materials 1 and 2 having equal z-direction indices $n_{1z} = n_{2z}$ ($\Delta n_z = 0$), Eq. 1 reduces to

$$r_p = \frac{n_{2y} - n_{1y}}{n_{2y} + n_{1y}} \tag{6}$$

which is independent of angle (shown by curve e in Fig. 2).

For a broader class of materials, when the z-direction index difference $(n_{1z} - n_{2z})$ is nonzero and has the opposite sign from the in-plane index difference $(n_{1y} - n_{2y})$, the fractional bandwidth of a multilayer stack reflection band and its reflectivity can actually increase with angle of incidence. Also, consider the special case where the two sets of index differences in materials 1 and 2 are equal with opposite sign, and $n_{1y} = n_{2z}$, or $n_{2y} = n_{1z}$. Equation 1 then reduces to

$$r_p = -r_s \tag{7}$$

for all angles of incidence. A quarter-wave multilayer interference reflector constructed with this material combination has identical s- and p-polarization reflection bands at all angles.

Multilayer interference optics depend not only on the interfacial reflections but also on the phase thickness relations that govern coherent interference. For example, reflection bands centered about a given wavelength λ_0 develop from a multilayer stack composed of alternating materials of high and low index, where the phase thickness of each of the layers in the structure is $\lambda_0/4$. The center wavelength λ_0 for a reflection band follows from a simple relation:

$$\lambda_0 = 2(n_1^{phz} d_1 + n_2^{phz} d_2) \tag{8}$$

where d_1 and d_2 are the physical thicknesses and n_1^{phz} and n_2^{phz} are the effective phase thickness indices of each material. The effective indices that are used to determine the phase relations of birefringent materials are

$$n_{is}^{phz} = \sqrt{n_{ix}^2 - n_0^2 \sin^2 \theta_0} \tag{9}$$

for s-polarized light and

$$n_{ip}^{phz} = \frac{n_{iy}}{n_{iz}} \sqrt{n_{iz}^2 - n_0^2 \sin^2 \theta_0} \tag{10}$$

for p-polarized light (*21*). Equations 1 to 4 and 8 to 10 are sufficient to describe the optical behavior of reflection bands developed from multilayer interference stacks, whether they are composed of conventional isotropic materials or from materials exhibiting large optical birefringence.

Reflection band examples. Reflection bands have characteristic features that describe their optical behavior. A reflection band is positioned about a particular wavelength, the center wavelength (Eq. 8), and the bandwidth, which refers to the span of wavelengths of high reflectivity. These characteristics are determined by the interfacial reflectivity and phase thickness of the layers constituting the multilayer stack. Each of these has its own dependence on the incidence angle and polarization. The details of a multilayer stack structure (the sequence of unit cells) also affect reflection band characteristics. Generally, the greater the number of unit cells in a stack and the larger the index difference between adjacent layers, the greater the reflectivity at and around the center wavelength. The simplest reflection band designs use many repeats of identical unit cells. Other designs may use a sequence of unit cells that have a gradation of thicknesses so as to increase the overall bandwidth of the reflection band (*23*).

The reflection band characteristics of a pair of isotropic materials are compared to those for a hypothetical pair of birefringent materials in Fig. 3. The inset in Fig. 3A shows the material configuration, with the length of the arrows along the x, y, and z directions representing the magnitude of each material's indices along the respective directions. The magnitude of the reflection at the interface between materials 1 and 2 versus incidence angle for p-polarized and s-polarized incident light (Fig. 3A) for this pair of isotropic materials shows the typical behavior of interfacial reflection for p-polarized light. At 55°, the value of the Fresnel reflection drops to zero (θ_B) for light incident from an external medium with $n_0 = 1.4$. Figure 3B shows reflection bandwidth versus incidence angle for a tuned (quarter-wave at normal-angle incidence) interference stack composed of alternating layers of these isotropic materials 1 and 2. As incidence angle increases, the centers of the s-polarized and p-polarized reflection bands move to shorter wavelengths as the effective phase thickness of the layers decreases. The reflection band behavior is calculated using the four effective indices with the characteristic matrix method (*24*) and locates the band edges for a design with a large number of unit cells. In this instance, the reflection band edges are plotted. Note that the reflection band "disappears" for p-polarized light at the θ_B values for these isotropic material interfaces.

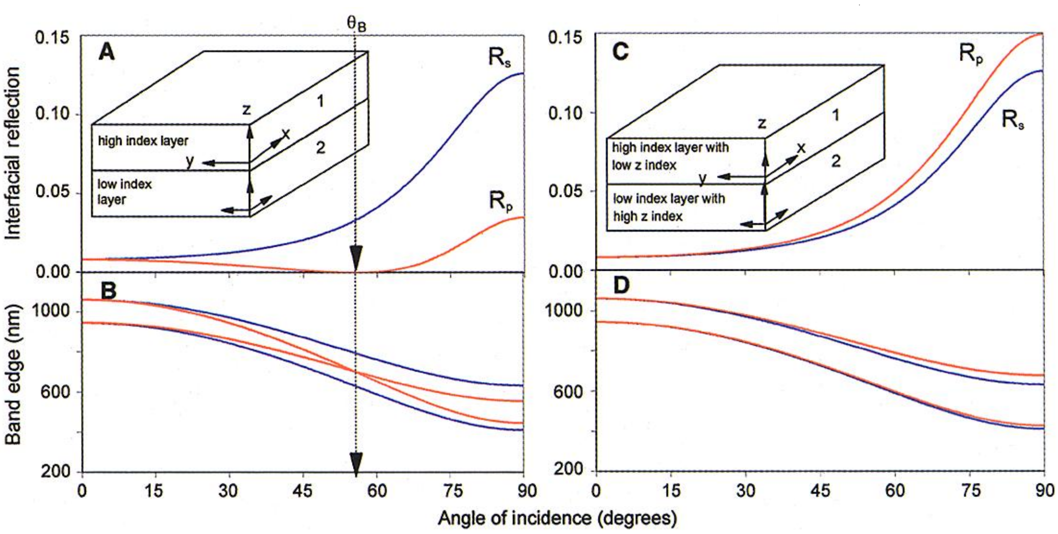

Fig. 3. Angular dependence of (**A** and **C**) interfacial reflection and (**B** and **D**) the long- and short-wavelength band edges for an isotropic layer pair and a GBO layer pair, respectively, of low and high in-plane indices of refraction. In (A), the p-polarization θ_B is near 55° and the reflection band disappears at that angle in (B). For (A) and (B), $n_{1x} = n_{1y} = 1.8$, $n_{1z} = 1.8$, $n_{2x} = n_{2y} = 1.5$, $n_{2z} = 1.5$, and $n_0 = 1.4$. For the GBO material pair, the low and high indices of refraction in the x-y plane have the opposite sign index difference compared with that along the z axis. In (C) and (D), the p-polarization reflection is higher than the s-polarization reflection with angle. For this GBO example, $n_{1x} = n_{1y} = 1.8$, $n_{1z} = 1.5$, $n_{2x} = n_{2y} = 1.5$, $n_{2z} = 1.9$, and $n_0 = 1.4$.

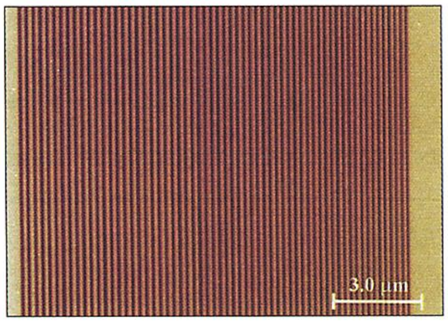

Fig. 4. An AFM image of a GBO stack (*31*); the dark-colored layers are PMMA and the light-colored layers are birefringent polyester (polyethylene naphthalate). Layers on the left side of the image are about 25% thicker than those on the right.

In Fig. 3, C and D, both materials 1 and 2 are birefringent. Material 1, with the higher in-plane index, is negatively birefringent; its z-direction index is lower and matched to the in-plane index of material 2. Material 2 is positively birefringent, with its z-direction index higher than its in-plane index and nearly matched to the in-plane index of material 1. As before, the external medium has an index of 1.4. In this instance, the Fresnel reflection of p-polarized light at the interface between materials 1 and 2 actually increases with incidence angle (Fig. 3C), much the way it does for s-polarized light. Figure 3D shows how the p-polarized light reflection band of a multilayer quarter-wave stack of these materials has an increasing fractional bandwidth with increasing incidence angle, in a manner nearly identical to the s-polarized light reflection band.

Another important parameter affecting the behavior of multilayer stack reflection bands is the relative phase thicknesses of the material components in a unit cell. A measure of relative phase thicknesses, termed the f-ratio, is the ratio of the phase thickness for each layer relative to the aggregate phase thickness of the repeating unit cell. It determines how the Fresnel reflections of each layer interface are coherently summed across the unit cells in the optical stack, which in turn determines reflection band behavior with changing incident angle. In many optical stack designs, suppression of higher order reflection bands (harmonics of the primary, first-order reflection band) is an important consideration (*25*). For p-polarized light, GBO provides an increased level of control of f-ratio with changing incidence angles. By using effective phase indices (Eq. 10), it can be shown that the f-ratio for a z-direction index-matched unit cell for p-polarized light is unchanged with angle. This control of the f-ratio can lead to pass-band designs (pass filters) that are very robust with incidence angle.

The reflection bandwidth of a multilayer interference mirror made from a sequence of repeated, identical unit cells is determined by the effective interfacial indices (Eqs. 3 and 4) of the materials and their f-ratios. To create a wider reflective band, a standard technique is to use a graded unit cell thickness profile. A 60–unit cell interference mirror with a 25% thickness gradient was fabricated from a birefringent polyester and polymethylmethacrylate (PMMA) [see, e.g., (*12, 26–28*) for optical properties]. A cross section of this multilayer interference structure was characterized with an atomic force microscope (AFM) (Fig. 4).

The layer thickness distribution developed from the AFM characterization was used in conjunction with measured dispersive values n_{1x}, n_{1y}, n_{1z}, n_{2x}, n_{2y}, and n_{2z} as input for a multilayer interference optical film model. These refractive index values were measured for thick monolithic films of both PMMA and birefringent polyester that had undergone the same film fabrication process as the multilayer mirror. These measurements indicate that the PMMA and birefringent polyester constituting the unit cells are matched in their z-axis refractive indices, with a substantial mismatch for their in-plane indices (GBO). Curve e in Fig. 2 shows the expected behavior of the interfacial reflectivity (p-polarized light) versus incidence angle for these GBO material interfaces.

The measured and calculated spectra for this mirror sample are compared in Fig. 5. For ease of comparison, optical density [essentially –log(1 – reflectance) for these low-loss, low-scatter polymers] is plotted. With the AFM-measured layer profile and dispersive refractive index values, the measured transmission spectra at normal incidence are well matched by spectra modeled using either the GBO refractive indices or isotropic refractive index values (set to the measured in-plane values). Using the same measured indices and layer thickness profile, the GBO calculations agree very well with 60° incidence (from air) p-polarization measurements, but the agreement is very poor for the isotropic refractive index calculation. Both the details of the reflection band and the band edge positions are faithfully reproduced with the model calculation incorporating the GBO refractive indices. Indeed, as expected for a GBO system with matched z-axis refractive indices, all of the characteristics of the normal incidence reflection band are maintained for high-incidence p-polarized light. Calculations using the isotropic refractive index values in the model result in a substantially weaker reflection band that is easily differentiated from the mirror using z-axis index-matched materials.

The refractive index values measured for the thick monolithic films of both PMMA and birefringent polyester are consistent with the GBO effects shown in Fig. 5 for the mirror sample with individual layer thicknesses ranging from 90 to 120 nm. This result supports recent work on the optical and physical properties of thin polymer layers (*29*).

Applications. The enhanced control of p-polarized light enabled by GBO allows different multilayer interference stack designs to be developed for numerous optical applications. GBO multilayer interference stacks can be fabricated with a variety of manufacturing methods. One economical method is polymer coextrusion (*11*). With this technique, we have produced a variety of optical films having between 100 and 1000 layers. With no rigid substrate, they are thin and flexible.

GBO broadband mirrors. As shown above (curve e in Fig. 2), a z-direction index-matched multilayer interference stack exhibits reflection band behavior for p-polarized light that enables previously unavailable performance. One optical application that can take advantage of this characteristic is a broadband mirror, intended to be an efficient transporter of visible light. The measured spectra in Fig. 6A illustrate the angular behavior of such a GBO broadband mirror containing 448 layers of birefringent polyester and PMMA. The normal incidence reflection spectrum is compared with the reflectance spectra measured for p-polarized light incident at 45° from air and from a glass prism. Note how the p-polarized light reflection stays very high at high incidence angle, particularly that demonstrated by the spectra for the mirror "immersed" in a glass medium.

Broadband mirror applications that use multibounce reflections are very sensitive to reflectivity levels and color changes upon reflection. Figure 7A shows a set of three circular cylinders, each of which is lined with a high-

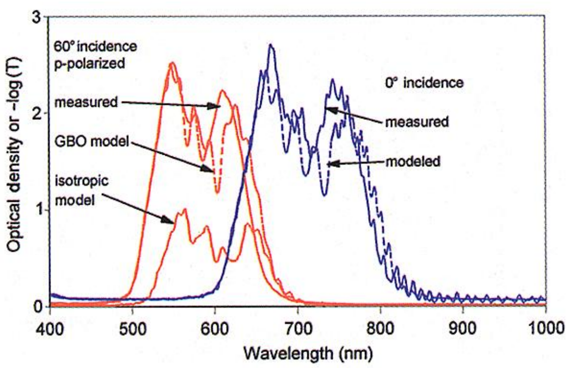

Fig. 5. Comparison of measured and modeled results for light transmission (T) at normal incidence and for 60° incidence of p-polarized light. The plot shows good agreement between measurements and high-incidence p-polarized GBO model calculations, and poor agreement for an isotropic materials calculation at high incidence angles with p-polarized light.

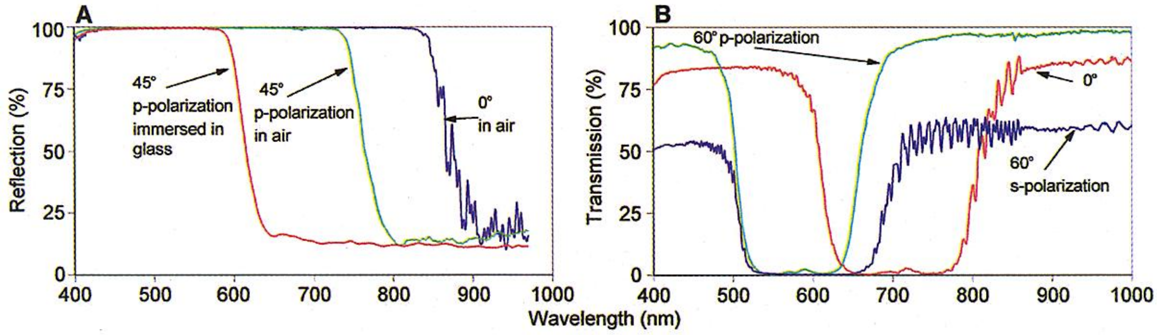

Fig. 6. (**A**) Measured broadband visible mirror reflection for various incidence angles. The p-polarized light measurements show no loss of reflection, only an increased band shift upon immersion in a glass incidence medium (n_0 = 1.52). (**B**) Measured spectrum for a GBO color mirror at normal and 60° angle of incidence, for s- and p-polarizations. In (A) and (B), the sequence of unit cells has a gradient in thickness to increase the reflection bandwidth.

reflectivity mirror. A broadband, "white" light source is obliquely illuminating each tube's entrance aperture. Tube a is lined with a multilayer GBO film with matched *z*-direction indices. Tube b is lined with a high-quality, second-surface aluminum mirror, and tube c is lined with a high-quality second-surface silver mirror. The light exiting each tube has undergone a large number of reflections across a range of high incidence angles. The resulting light intensity and color fidelity of the exiting light provide a measure of the level of omnidirectional reflection quality. As can be seen in the photograph, the light exiting the GBO broadband mirror tube has both high intensity and good color fidelity. The silver mirror tube shows an obvious "yellowing" of the exit light, and the aluminum tube has markedly lower exit-light intensity.

GBO color mirrors. A nonpolarizing color mirror that operates over a range of incidence angles and wavelengths is a difficult task for a designer using conventional optical materials (*30*). For non-normal incidence, polarization effects limit band edge sharpness, which can greatly affect color purity. GBO techniques can be used to construct a color mirror that has a matched band edge at all angles for both p- and s-polarized light, eliminating these difficulties.

The importance of the use of GBO for color mirrors is illustrated in the following example. Transmission spectra for a GBO stack with all layers having matched *z*-direction indices near 1.5 are shown in Fig. 6B. Measurements for normal incidence and 60° angle of incidence for s- and p-polarized light are shown. Note that the small midband leak at normal incidence is reproduced with its intensity unchanged in the 60° p-polarization measurement. Because the air-polymer interface does not meet GBO criteria, typical Brewster's law behavior is observed for wavelengths outside the reflective band (transmission levels of 60% for s-polarization and 98% for p-polarization). Although the long-wavelength band edges are substantially different, the short-wavelength band edges for s- and p-polarization are nearly identical.

The range and intensity of colors that are created in a film cavity made of these materials is shown in Fig. 7B. In this photograph, the cavity is externally illuminated with a "white" light. The multiple bounces produced in a cavity with high reflectivity over a portion of the visible spectrum accentuate the reflected intensity variation at different wavelengths, creating intense color. The highly saturated colors seen at all observation angles are a result of the matched s- and p-polarization band edges at all angles, combining light transmitted through and reflected from the cavity surfaces.

GBO reflective polarizers. GBO multilayer interference stacks can be fabricated with a high refractive index difference developed along only one in-plane axis, creating a reflecting polarizer. A schematic of a unit cell with appropriate indices is shown in Fig. 8A, indicating a biaxial refractive index for at least one of the layers. Figure 8B shows reflection measurements along the two principal axes (see Fig. 1). With the use of GBO techniques, the ultimate omnidirectional reflective polarizer can be made where the index differences between layers are zero along both the *x* and *z* axes. In such a system, light polarized along the reflective axis (*y* direction) behaves according to curve e in Fig. 2 for p-polarized light. For light polarized along the

A

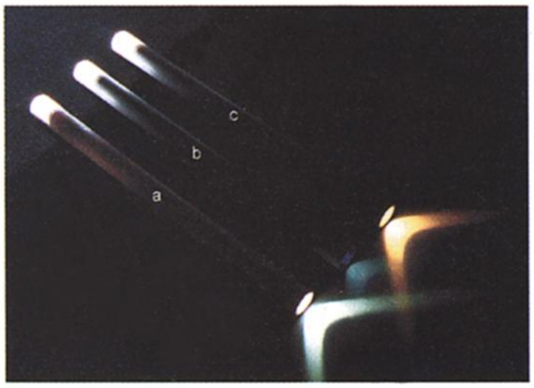

B

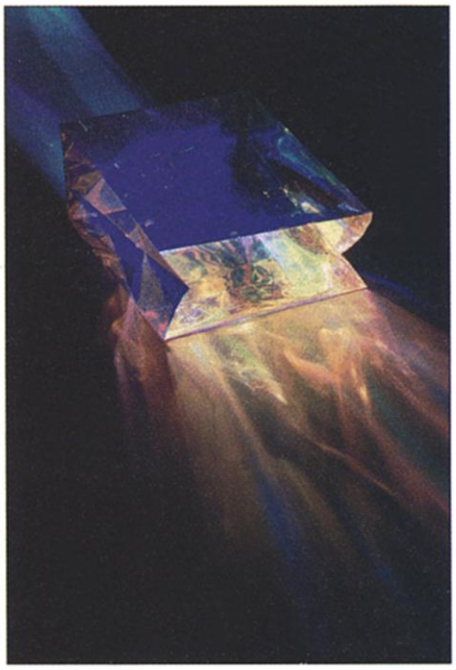

Fig. 7. (**A**) Light transport tubes using (a) GBO broadband mirror, (b) commercial aluminum mirror, and (c) commercial silver mirror. The ratio of length to diameter of the tubes is 17, and white light is used to illuminate the open aperture. (**B**) A GBO film cavity that is illuminated from the front aperture with white light. Note the change of highly saturated color with observing angle.

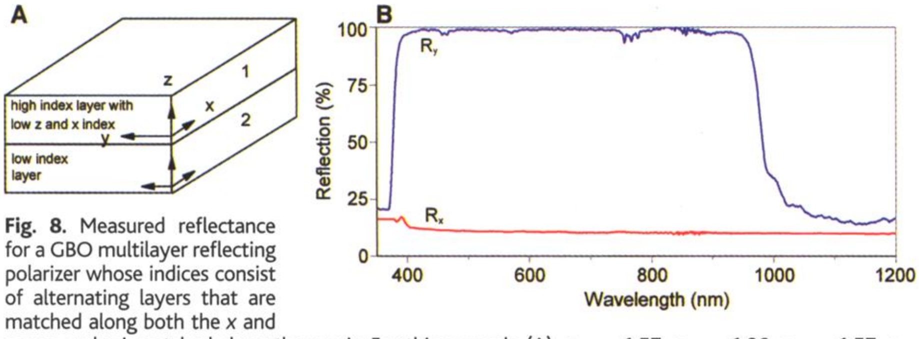

Fig. 8. Measured reflectance for a GBO multilayer reflecting polarizer whose indices consist of alternating layers that are matched along both the x and z axes and mismatched along the y axis. For this example (**A**), n_{1x} = 1.57, n_{1y} = 1.86, n_{1z} = 1.57, n_{2x} = 1.57, n_{2y} = 1.57, n_{2z} = 1.57, and n_0 = 1.0. (**B**) When measured in the y direction, reflection shows a strong band at near 100% intensity. Along the x direction, there are only air interface reflections.

pass axis (x direction), neither s- nor p-polarized light is reflected by the multilayer stack for any angle of incidence, as the relevant index differences are zero.

Although more complex than a mirror with uniaxial symmetry, GBO design concepts for reflective polarizers can be applied separately for light polarized along each axis. The Fresnel and phase thickness equations given above hold for light incident with its polarization direction parallel to either the x axis or y axis. Reflective polarizers constructed with the polymers discussed above have a demonstrated extinction ratio of 300:1 averaged across all visible wavelengths at all angles of incidence.

References and Notes

1. P. Baumeister and G. Pineus, *Sci. Am.* **223**, 58 (December 1970).
2. P. Drude, *Wied. Ann.* **43**, 146 (1891).
3. ______, *Ann. Phys. Chem.* **38**, 865 (1891).
4. D. Brewster, *A Treatise on Optics* (Lea & Blanchard, London, 1839).
5. M. Banning, *J. Opt. Soc. Am.* **37**, 792 (1947).
6. P. Lissberger, *Rep. Prog. Phys.* **33**, 197 (1970).
7. V. R. Costrich, *Appl. Opt.* **9**, 866 (1970).
8. A. Thelen, *Appl. Opt.* **15**, 2983 (1976).
9. ______, *J. Opt. Soc. Am.* **70**, 118 (1980).
10. T. Ito, U.S. Patent 5,579,159 (26 November 1996).
11. T. Alfrey, E. F. Gurnee, W. J. Schrenk, *Polym. Eng. Sci.* **9**, 400 (1969).
12. C. J. Heffelfinger and K. L. Knox, *The Science & Technology of Polymer Films* (Interscience, New York, 1971), p. 587.
13. D. A. Holmes and D. L. Feucht, *J. Opt. Soc. Am.* **56**, 1763 (1966).
14. R. M. A. Azzam and N. M. Bashara, *Ellipsometry and Polarized Light* (Elsevier, Amsterdam, 1987), p. 119.
15. D. W. Berreman, *J. Opt. Soc. Am.* **62**, 502 (1972).
16. P. Yeh, *J. Opt. Soc. Am.* **69**, 742 (1979).
17. I. Hodgkinson and Q. H. Wu, *J. Opt. Soc. Am. A* **10**, 2065 (1993).
18. J. Lekner, *J. Opt. Soc. Am. A* **10**, 2059 (1993).
19. Y. Fink *et al.*, *Science* **282**, 1679 (1998).
20. Optical stack designs with isotropic materials often compensate for this reduction of p-polarization reflectivity with incidence angle by increasing the number of unit cells in the multilayer stack to such a level that the reflectivity falloff is minimized. This approach can be quite successful for isotropic multilayer interference layers with air as the external medium, but has limited utility when the external medium allows for larger propagation angles to be present in the stack.
21. R. M. A. Azzam and N. M. Bashara, in (*14*), p. 357 (corrected equation).
22. M. Born and E. Wolf, *Principles of Optics* (Pergamon, New York, ed. 5, 1975), p. 40.
23. O. S. Heavens and H. M. Liddel, *Appl. Opt.* **5**, 373 (1966).
24. M. Born and E. Wolf, in (*22*), p. 66.
25. A. Thelen, *J. Opt. Soc. Am.* **53**, 1266 (1963).
26. J. C. Kim, M. Cakmak, X. Zhou, *Polymers* **39**, 4225 (1998).
27. J. C. Seferis, *Polymer Handbook* (Wiley, New York, ed. 3, 1989), p. 45.
28. M. Cakmak and J. L. White, *Polym. Eng. Sci.* **29**, 1534 (1989).
29. R. L. Jones, S. K. Kumar, D. L. Ho, R. M. Briber, T. P. Russel, *Nature* **400**, 146 (1999).
30. H. A. Macleod, *Thin-Film Optical Filters* (Macmillan, New York, ed. 2, 1986), p. 334.

31. AFM image and layer thickness analyses were provided by V. W. Jones of 3M Corporate Analytical Technology Center.

25 October 1999; accepted 15 February 2000

Dynamic Variations at the Base of the Solar Convection Zone

R. Howe,[1]* J. Christensen-Dalsgaard,[2] F. Hill,[1] R. W. Komm,[1] R. M. Larsen,[3] J. Schou,[3] M. J. Thompson,[4] J. Toomre[5]

We have detected changes in the rotation of the sun near the base of its convective envelope, including a prominent variation with a period of 1.3 years at low latitudes. Such helioseismic probing of the deep solar interior has been enabled by nearly continuous observation of its oscillation modes with two complementary experiments. Inversion of the global-mode frequency splittings reveals that the largest temporal changes in the angular velocity Ω are of the order of 6 nanohertz and occur above and below the tachocline that separates the sun's differentially rotating convection zone (outer 30% by radius) from the nearly uniformly rotating deeper radiative interior beneath. Such changes are most pronounced near the equator and at high latitudes and are a substantial fraction of the average 30-nanohertz difference in Ω with radius across the tachocline at the equator. The results indicate variations of rotation close to the presumed site of the solar dynamo, which may generate the 22-year cycles of magnetic activity.

The differential rotation of the sun and its ability to generate large-scale magnetic fields through cyclic dynamo action appear to be intimately linked. It is thought that the global dynamo behavior (*1*) responsible for the emergence of large active regions (sunspot groups) is derived from strong organized toroidal magnetic fields generated by rotational shear in a thin region, called the tachocline, at the base of the convection zone. The evolving magnetic field could well have a feedback effect on the fluid motion in that region. We are thus motivated to use helioseismology to look for changes in rotation profiles near the tachocline as the sun's magnetic cycle progresses. Here, we present evidence that the rotation rate in the interior changes with time, with unexpected periods of ~1.3 years near the equator and possibly 1.0 year at high latitudes.

Helioseismology provides the means to probe the interior structure and dynamics of the sun, using precise observations of the modes of oscillation (*2*). In particular, the splitting of the global oscillation frequencies by large-scale flows has successfully

[1]National Solar Observatory, National Optical Astronomy Observatories, Post Office Box 26732, Tucson, AZ 85726–6732, USA. [2]Theoretical Astrophysics Center, Danish National Research Foundation, and Institute of Physics and Astronomy, Aarhus University, DK–8000 Aarhus C, Denmark. [3]Hansen Experimental Physics Laboratory, HEPL Annex, Stanford University, Stanford, CA 94305–4085, USA. [4]Astronomy Unit, Queen Mary and Westfield College, University of London, Mile End Road, London E1 4NS, UK. [5]JILA and the Department of Astrophysical and Planetary Sciences, University of Colorado, Boulder, CO 80309–0440, USA.

*To whom correspondence should be addressed. E-mail: rhowe@noao.edu